ELSEVIER

Journal of Marine Systems 36 (2002) 219–238

JOURNAL OF MARINE SYSTEMS

www.elsevier.com/locate/jmarsys

Numerical investigation of the Sicily Channel dynamics: density currents and water mass advection

Anne Molcard [a,b,*], Liliana Gervasio [a], Annalisa Griffa [a,b], Gian Pietro Gasparini [a], Laurent Mortier [c], Tamay M. Özgökmen [b]

[a] *IOF-CNR, La Spezia, Italy*
[b] *RSMAS/MPO, University of Miami, Miami, FL, USA*
[c] *LODYC-CNRS/ENSTA, Paris, France*

Received 20 June 2001; accepted 29 May 2002

Abstract

The Sicily Channel connects the western and eastern Mediterranean sub-basins, playing a fundamental role in the dynamics of the Mediterranean circulation. The flow in the Channel is driven by direct forcing such as wind and by thermohaline processes leading to density difference between the two sub-basins. Assessing the relative role of these two types of forcing mechanisms is still an open question in the literature, despite its importance for a correct understanding and prediction of the Channel circulation. In this paper, we isolate the remotely forced, density-driven component of the circulation, considering a simplified setting, where the forcing is schematized as an imposed density difference along the channel, $\Delta\rho$. The study is carried out considering results from a high resolution numerical model of the circulation in the Channel area. A range of values for $\Delta\rho$ is considered, and the effects of changing $\Delta\rho$ on the circulation patterns, transport values and water mass advection are studied.

The patterns of the average circulation and water mass advection remain qualitatively similar at varying $\Delta\rho$. The simulations reproduce a number of realistic circulation features for both the surface Modified Atlantic Water (MAW) and the Levantine Intermediate Water (LIW). These include the complex branching patterns of the MAW at the entrance of the Channel, and the appearance of the characteristic structure of the Atlantic Ionian Stream (AIS) inside the Channel. At a more detailed level, the nonlinearity at increasing $\Delta\rho$ appears to influence some aspects of the circulation, such as the relative strength of the Tyrrhenian and Sicilian MAW branches.

The transport across the Channel is found to increase approximately linearly with $\Delta\rho$ in the considered range, with values ranging from ≈ 0.3 to ≈ 0.8 Sv. The lowest value corresponds to $\Delta\rho$ based on climatological density value in the neighbouring regions (Sardinia Channel and Ionian Sea), while the highest values correspond to more remote density values, i.e. to differences between the far-field western and eastern Mediterranean sub-basins.

Keywords: Water balance; Current; Numerical model; Sicily Strait

* Corresponding author. IOF-CNR, Forte Santa Teresa, 19036 Pozzuolo di Lerici (SP), Italy. Tel.: +39-0187-978302; fax: +39-0187-970585.

E-mail address: molcard@iof.cnr.it (A. Molcard).

0924-7963/02/$ - see front matter
PII: S0924-7963(02)00188-4

1. Introduction

The Sicily Channel connects the Eastern and Western Mediterranean Sea, playing an important role in the dynamics of the Mediterranean general circulation. At first approximation, the flow through the Sicily Channel can be considered as a two-layer system, in which the surface water of Atlantic origin, characterized by minimum salinity (Modified Atlantic Water, MAW), flows eastward, and the Levantine Intermediate Water (LIW), characterized by maximum salinity, flows westward underneath. Basic knowledge on the main current patterns is provided by observations (e.g. Astraldi et al., 1996, 1999; Malanotte-Rizzoli et al., 1997; Manzella et al., 1988, 1990; Moretti et al., 1993; Robinson et al., 1999; Sparnocchia et al., 1999), even though less numerous than in the other main strait of the Mediterranean Sea, namely the Gibraltar Strait (e.g. see Pratt, 1990 for a review). A schematic illustration of the circulation and of the water mass pathways, as indicated by the measurements in this region is shown in Fig. 1.

The MAW (Fig. 1a) flows from the Western Mediterranean along the Algerian coast and bifurcates at the Channel level: one branch, carrying about 1/3 of the incoming transport, crosses the Channel and continues eastward in the Tyrrhenian Sea along the northern coast of Sicily, while the other branch, carrying approximately 2/3 of the transport, enters into the Channel. The path of the latter is variable in time, and this branch is possibly subject to additional branching. Signatures of minimum salinity are found close to the Tunisian coast at the entrance of the Channel (Astraldi et al., 1996). The subsequent path is not known exactly because direct measurements are not available on the southern Tunisian shelf. The MAW is also found entering the Channel along the Sicilian coast and in the center of the Channel, which suggests the presence of a secondary branching (shown by the dashed line in Fig. 1a). Independently from the exact entrance point, a consistent vein of the MAW, often indicated as the Atlantic Ionian Stream (AIS), appears to reach the Sicilian shelf north of Malta, subsequently following the shelf and reaching the Ionian Sea. Robinson et al. (1999) underline the presence of some permanent structures in the path of the AIS.

The LIW (Fig. 1b) enters the Channel from the adjacent Ionian Sea, from the eastern side. Even

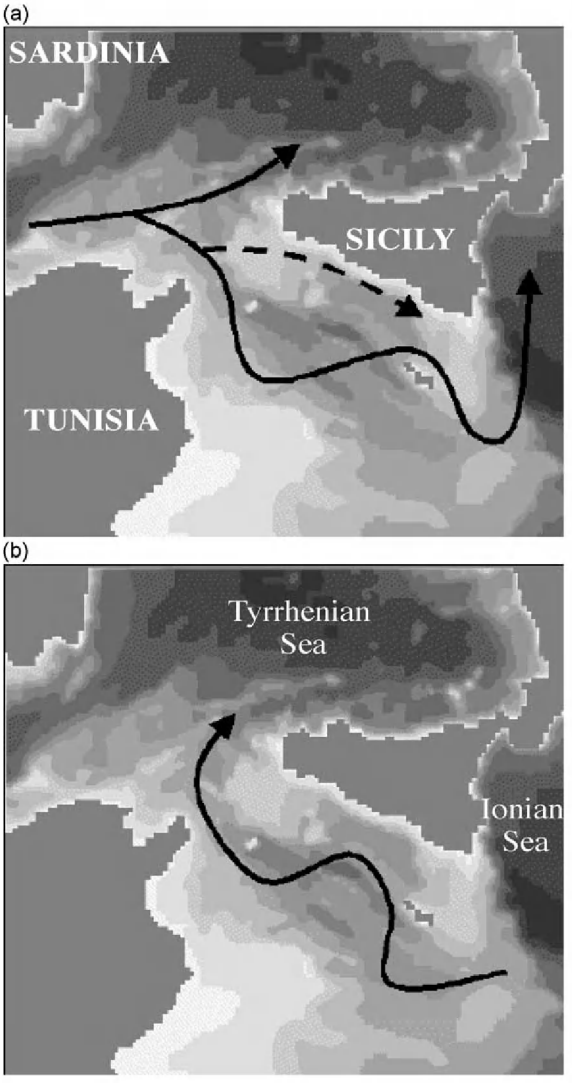

Fig. 1. The study area with the model bathymetry and the schematic pathways of (a) the MAW and (b) the LIW.

though the LIW occupies most of the Channel below a depth of 200 m, its main salinity core is observed to lay close to the Sicilian shelf, suggesting a position for the main current. The LIW flows out of the Channel over two main sills in the western side. After that, it appears to flow mostly eastward following the Tyrrhenian coast (Astraldi et al., 1996).

The mass flux crossing the Channel is estimated from observations to have a mean value on the order of 1 Sv, but with a high variability. Geostrophic

computations using hydrographic transects crossing the Channel yield values ranging from 1.15–1.23 Sv (Garzoli and Maillard, 1979) to 0.37–0.41 Sv (Moretti et al., 1993). Long-term current measurements indicate a mean transport of 1.1 Sv during the period 1993–1997 with a standard deviation of 0.58 Sv (Astraldi et al., 1999).

Dynamical forcing mechanisms in the Channel include both *local* atmospheric forcings such as wind and buoyancy fluxes and also *remote* forcing, mostly related to thermohaline processes leading to density differences between the western and eastern Mediterranean sub-basins. Assessing the relative role of these two types of forcing mechanisms is still an open question in the literature, despite its importance for a correct understanding and prediction of the Channel circulation. Results from direct observations (e.g. Astraldi et al., 1999) and from general circulation models (e.g. Horton et al., 1997; Korres et al., 2000) provide information on the overall characteristics of the circulation, but they cannot be used directly to separate the effects of various forcing mechanisms. Considerations based on salt and mass conservation suggest the relevance of the thermohaline remote forcing, yielding a thermohaline transport in the Strait of approximately 1 Sv (Bethoux, 1979; Hopkins, 1999), while model results tend to indicate the relevance of the wind stress in determining the flux values (Heburn, 1994; Korres et al., 2000). Regional modeling studies (Onken and Sellshop, 1998; Pierini and Rubino, 2001) do not provide a direct insight on the nature of the forcing, since they investigate the onset of circulation and instabilities for specified values of incoming fluxes.

The objective in this study is to investigate how much of the circulation patterns in the Sicily Channel region can be captured by using an idealized, local model with thermohaline forcing only. A simplified setting is considered, where the forcing is schematized as a boundary forcing, characterized by an imposed density difference along the channel, $\Delta\rho$. Using this simple model, we address the following questions: can thermohaline forcing alone generate anything like what is seen in the observations, or something quite different? If it generates circulation patterns resembling those from observations, how much forcing at the boundaries is needed to do so? How do the interior patterns and the transport through the Channel vary as a function of the boundary forcing? What is the reasonable range of boundary forcing, or equivalently of $\Delta\rho$, required to induce the observed level of Channel transport? Which observed circulation patterns cannot be captured and cannot be explained using boundary thermohaline forcing only? It will be therefore deduced indirectly which circulation patterns require other forcing mechanisms, such as wind forcing and the use of more sophisticated models.

A process study is performed varying the strength of the forcing and studying the response of the system through numerical integration of a high resolution circulation model of the Channel area, with realistic topography. A similar approach has been previously followed in other papers (Herbaut et al., 1996, 1998; Gervasio et al., submitted for publication), focusing on analytical and numerical spin-up solutions of simplified models. Here we consider the longer time evolution of the system, with special interest in transport and water mass properties.

Results from three main numerical experiments are presented in detail. They focus on the effects of surface density difference across the Channel, and cover a realistic range of climatological $\Delta\rho$ values. The effects of changing $\Delta\rho$ on the circulation patterns, water mass advection and transport values are studied. A comparison is performed between transport values obtained from the circulation model, and bulk estimates obtained using the simplified steric height methods (Hopkins, 1999). The method is also used to investigate the effects of the (smaller) density difference occurring in the intermediate layer.

The paper is organized as follows. In Section 2, the numerical model and the configuration of the experiments are discussed, while the results are presented in Section 3. In Section 4, the comparison with the results using the steric height method is shown. A summary of this study and conclusions are provided in Section 5.

2. Numerical model, configuration and forcing representation

Numerical experiments are performed using OPA7 (Ocean Parallel), a finite difference primitive equation model originally developed at Lodyc. The model is

well documented in the literature, and the reader is referred to Andrich et al. (1988) and Madec et al. (1991a,b) for a review of the details of this model. The version utilized in the present study is subject to rigid-lid and hydrostatic approximations, and employs a z-coordinate system for vertical discretization. Subgrid-scale physics is parameterized by a fourth-order operator for momentum and tracers. The horizontal eddy viscosity and diffusion coefficients are equal to 10^9 m^4 s^{-1} (as we use a bi-Laplacian operator) and the vertical coefficients are assumed to vary as a function of the local Richardson number according to the parameterization proposed by Pacanowski and Philander (1981).

The computational domain, shown in Fig. 2, extends between 33.0°N and 40.0°N in latitude and between 7.0°E and 18.0°E in longitude. The bottom topography (Fig. 1) is derived from International Bathymetric Chart of the Mediterranean (IBMC) with a spatial resolution of 1/100°. No-slip boundary conditions are applied along the coasts. Open sea boundaries are treated as closed, but they are outfitted with buffer zones, that provide a crude representation of the action of the external basins that are not explicitly included. In these restricted damping zones, model temperature and salinity fields are restored to their initial values, while velocity is damped locally by increasing the viscosity.

The horizontal grid is defined on a Mercator projection with a resolution of $1/16° \times 1/16° \cos\theta$, corresponding to an average grid size of approximately 5 km. The vertical density structure is represented by 43 z-levels, with a resolution varying from 3 m near the surface to 200 m near the bottom, using a transition function (hyperbolic tangent) between levels.

The forcing is designed to schematically represent the effects of different density structures in the two sub-basins connected by the Channel. This density differences drive "remotely" the current in the local

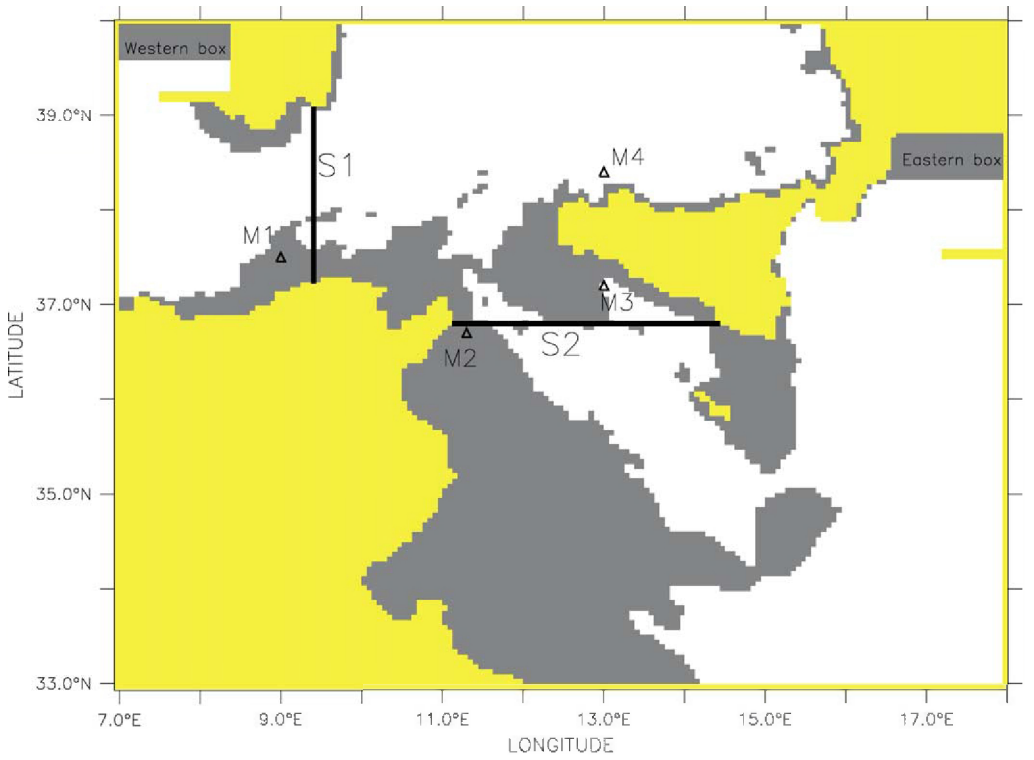

Fig. 2. Numerical domain with the 350 m bathymetry showing the forcing boxes, the sections denoted S1 and S2 for the transport computations, and the points marked M1, M2, M3, M4 to follow the advection of the MAW.

Table 1
Densities values in the surface, intermediate and bottom layers for experiments DG1, DG2 and DG3

Box1	Interior	Box2
DG1		
27.19	27.57	27.96
29.07	29.07	29.07
29.09	29.09	29.09
DG2		
26.81	27.57	28.34
29.07	29.07	29.07
29.09	29.09	29.09
DG3		
26.42	27.57	28.72
29.07	29.07	29.07
29.09	29.09	29.09

The "box" densities are kept fixed, whereas the "interior" density corresponds to that at the initial time. The thicknesses of the surface, intermediate and bottom layers are 150, 450, and 3500 m, respectively.

Channel area, through the propagation of the so-called Kelvin fronts (e.g. Herbaut et al., 1998). In a number of previous papers, (e.g. Herbaut et al., 1996, 1998; Gervasio et al., submitted for publication), this remote forcing has been studied using a simplified setting where the sub-basins are schematically represented by "boxes", where the density profiles and the associated gradients with ambient waters are maintained constant. Conceptually, these boxes represent the reservoir of available potential energy contained in the sub-basins and act as "motor" for the system. The same framework is used in the present paper.

In the numerical experiments presented in Section 3, the forcing boxes are situated as shown in Fig. 2. The western box is located in the northwestern corner of the domain near Sardinia, and it characterizes the inflowing MAW with relatively low density. The eastern box is situated in the northeast region, in the denser Ionian Sea, and characterizes the AIS outflowing from the basin. In preliminary experiments, the sensitivity to the specific box location and size has been studied. In particular, the latitudinal extent of the eastern box has been modified, up to cover the whole eastern boundary. The results in terms of circulation and transport in the Channel are found to be quite insensitive (see Section 3.1 for details).

The density profiles in the boxes are idealized to characterize a three-layer system (Table 1). Three main experiments are considered, DG1, DG2, DG3. They focus on the surface density difference (approximately upper 150 m), which is more than an order of magnitude bigger than the differences in the lower levels (see Section 4). The densities of the intermediate and deep layers are assumed to be the same in the three experiments as well as in the two boxes and in the initial basin stratification. In this setting, then, the forcing is provided by the surface gradient which determines a baroclinic current with a surface component representing the MAW and an intermediate component representing the LIW. This choice of the forcing is of course a crude simplification of reality, but it allows to isolate the effects of the main forcing function. The effects of intermediate density differences is investigated using the steric height method in Section 4.

The three runs are characterized by increasing surface density difference between the two boxes, $\Delta\rho = 0.77$, 1.53, 2.30 for DG1, DG2 and DG3, respectively (Table 2), corresponding to a factor of 2 between DG1 and DG2 and to a factor 3 between DG1 and DG3. The lowest $\Delta\rho$ (DG1) corresponds to differences between climatological density (Brasseur et al., 1996; Guibout, 1987) in the neighbouring regions (Sardinia Channel and Ionian Sea), while the highest $\Delta\rho$ (DG3) corresponds to differences between the far-field western and eastern Mediterranean (approximately corresponding to the Alboran Sea and the Levantine basin). An intermediate $\Delta\rho$ value is chosen for DG2.

The density profiles defined in the two boxes are maintained throughout the integrations, as well as

Table 2
Values of density differences between the two boxes, $\Delta\rho$, volume transports in Sv (mean ± standard deviation) across sections S1 and S2 (see Fig. 2) and their ratios (multiplied by 3), for experiments DG1, DG2 and DG3

	DG1	DG2	DG3
$\Delta\rho$	0.77	1.53	2.30
S1	0.47 ± 12%	0.92 ± 21%	1.39 ± 15%
S2	0.31 ± 17%	0.53 ± 21%	0.810 ± 19%
S3	0.16	0.39	0.58
3 × S3/S1	1.02	1.27	1.25
3 × S2/S1	1.98	1.73	1.75

their gradients with the ambient waters, by constant linear relaxation of the corresponding temperature and salinity profiles toward the initial values (using a relaxation coefficient of 1 day). In all the three runs, the rest of the domain is initialized with a surface Mediterranean density corresponding to the average of the two box values to guarantee that the density gradient is the same for the two boxes. This "central Mediterranean" density profile is let free to evolve according to the model dynamics. The time step used in the numerical integration ranges from 14 min for experiments DG1 and DG2, to 7 min for DG3.

3. Results from numerical experiments

In the following, the results of the three experiments DG1, DG2 and DG3 are presented. First, the basic mechanisms of the first spin-up phase are briefly reviewed. Then, the characteristics of the solutions are illustrated with emphasis on the general circulation patterns, water-mass advection characteristics and transports at selected sections. Notice that the first spin-up phase (Section 3.1) is not realistic, since it depends on the artificial initial condition. Nevertheless, as shown in a number of previous papers, (e.g. Herbaut et al., 1996, 1998; Pierini and Rubino, 2001), this phase can be of interest because it provides some understanding of the circulation setting and it allows to isolate and separetely study the role of the various boundary forcings. Also, the results are relevant to the understanding of transients due to time dependent perturbations of the forcings, such as for periods following intense dense-water formation elsewhere in the Mediterranean basin.

3.1. First spin-up phase

The first phase of the spin-up is very similar for all three experiments, and is dominated by the set-up of coastal currents generated by incident Kelvin fronts due to density gradients (Speich et al., 1996). At the initial time, in fact, the "gates" of the two boxes (Fig. 2) are opened, and a current system is set up by the density gradients. For the configuration in Fig. 2, the solution is expected to be due to the superposition of two Kelvin fronts, generated by the western and eastern box, respectively. In order to illustrate the role of each box, we have first performed a preliminary experiment considering the action of each box separetely. The results are shown in Fig. 3 for DG3.

The gradient in the western box, where surface water is lighter, generates a Kelvin front flowing eastward along the Tunisian coast and sets an eastward surface current (Fig. 3a). At the Channel entrance (Herbaut et al., 1998), a barotropic and baroclinic double Kelvin wave associated to the shelf break north of the Channel causes the front to separate, generating two main surface current branches. One branch enters the Channel and flows south along the Tunisian coast, whereas the other branch crosses the Channel and reaches the Tyrrhenian Sea.

The front induced by the eastern box, instead, is characterized by denser surface water. It propagates along the Sicilian coast (Gervasio et al., submitted for publication), keeping the coast to its right, while generating a surface coastal current moving in the opposite direction, i.e. southeastward in the Channel toward the box (Fig. 3b). This current connects the Tyrrhenian and the Ionian Sea, flowing along the Sicily coast through the Channel and then northward in the Ionian Sea.

When both boxes are active, the two fronts and the associated currents joint to set up the basin circulation (Fig. 4c). The current pattern shows the main MAW bifurcations and the typical pattern of the AIS. Notice that the solution in Fig. 4c corresponds almost exactly to the linear superposition of the two solutions in Fig. 3a,b, indicating that the dynamics in this phase is in good approximation linear. This is shown also by the striking resemblance of the flow patterns for the various experiments (see Fig. 4a for DG1), after the same integration time. The preliminary experiments indicate that the MAW branching and the setting of the Tunisian current are mostly related to density differences with the western basin, while the northward current in the Ionian sea and the AIS pattern are mostly due to differences with the eastern basin.

The time scale of this first spin-up phase is related to the time necessary for the Kelvin front to circulate around the basin. This phase speed depends primarily on the vertical initial basin stratification (Herbaut et al., 1998), which is the same for all the experiments, and it is on the order of 1 m s^{-1}. The spin-up phase, then, is expected to last less than 20 days, as confirmed by the numerical results. The current patterns

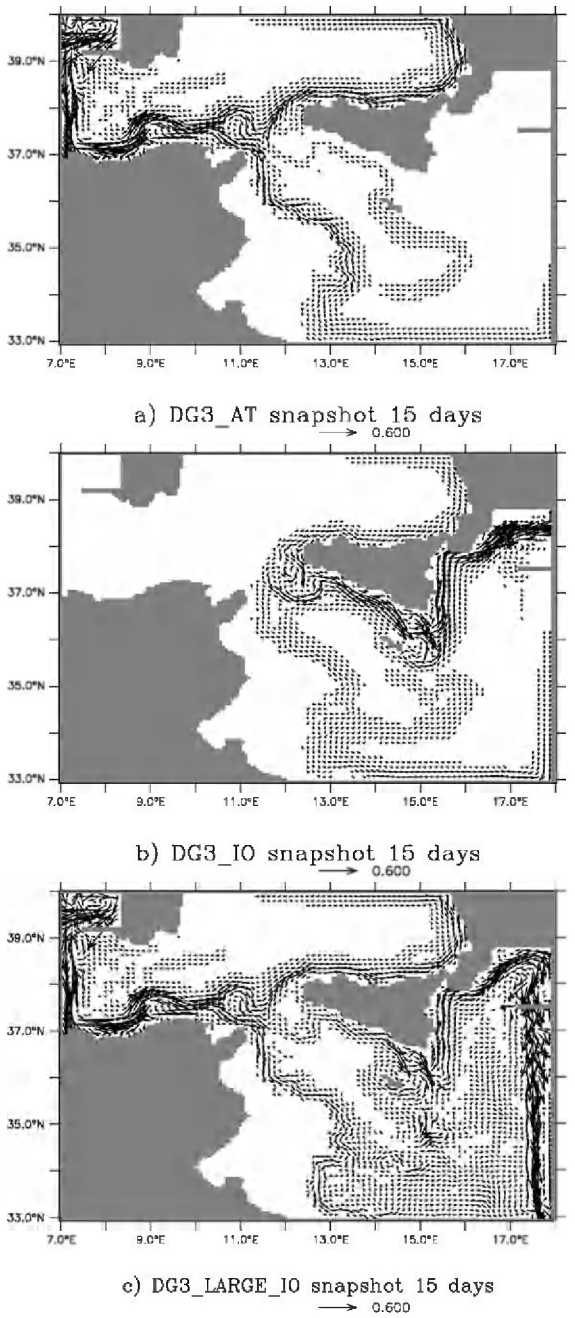

Fig. 3. Snapshots of surface velocity (in m s^{-1}) for experiment DG3 at 15 days with (a) only the western box, (b) only the eastern box and (c) with the western box and an eastern box covering the whole eastern boundary.

in Figs. 3 and 4a–c, in fact, are obtained at $t=15$ days.

It is interesting to note that results analogous to those in Fig. 3 are obtained also when the box shape is changed, for example increasing the latitudinal extent of the eastern box (as already mentioned in Section 2). Results at $t=15$ days for an eastern box covering the whole eastern boundary are shown in Fig. 3c. The circulation ouside from the box is equivalent to the circulation in Fig. 4c, and also the transport values across the Strait are the same. Similar results have also been reported by Pierini and Rubino (2001), using a different model setting. In Pierini and Rubino (2001), the circulation in the Sicily Channel is forced by prescribed transports uniformely distributed along two prescribed sections at the two opposite sides of the Channel. The spin-up circulation is dominated by Kelvin fronts propagating along the coasts and leads to localized currents, which are very similar to those in Fig. 4a–c. This indicates generality of the results with respect to specific configurations.

3.2. Subsequent evolution and time-averaged velocity fields

After the first spin-up phase, the solution enters a second phase of evolution dominated by the advection of the low density MAW in the basin. The time scale of this phase is related to current advection, and it is expected to be significantly longer since the advection velocity is significantly smaller than the Kelvin front phase speed. The results relative to the circulation in this phase are shown here for the three experiments, starting from DG1, characterized by the lowest density difference $\Delta\rho$ (Table 1).

The DG1 experiment is integrated for a total time of 3.5 years. A first characterization is given by the evolution of the density integrated over the whole basin in the upper layer, where the MAW is advected:

$$\rho_D(t) = \frac{\int_A \mathrm{d}x\mathrm{d}y \int_0^{-D} \mathrm{d}z\rho(x,y,z,t)}{\int_A \mathrm{d}x\mathrm{d}y \int_0^{-D} \mathrm{d}z}. \quad (1)$$

In Eq. (1), A is the horizontal basin domain, $z=0$ is the surface level and D is a prescribed depth of integration in the upper layer. Results showing the

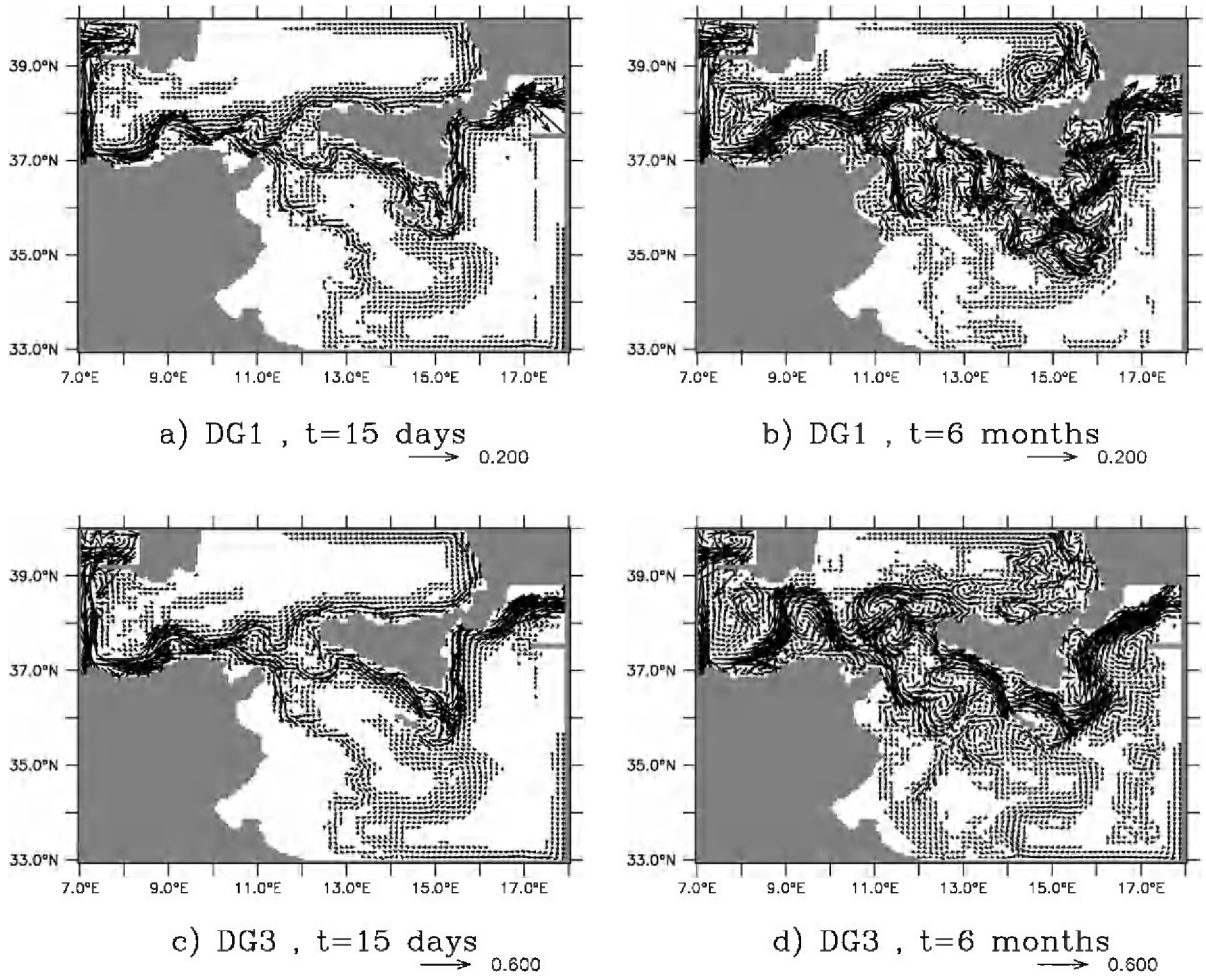

Fig. 4. Snapshots of surface velocity (in m s^{-1}) for (a) the experiment DG1 at 15 days (b) the experiment DG1 at 6 months, (c) the experiment DG3 at 15 days, and (d) the experiment DG3 at 6 months.

evolution of $\rho_D(t)$ for $D=15$ m, i.e. for shallow integration, are shown in Fig. 5a. Similar results are found for D up to approximately 55 m. For $D>55$ m, oscillations start to occur due to the motion of the interface between different water masses (Table 1). The behavior of ρ_D (Fig. 5a) indicates that the simulation has not yet reached a complete equilibrium at the end of the integration period of 3.5 years. The most noticeable changes, though, occur during the first 2 years, as shown also by the MAW advection patterns discussed in Section 3.3.

During this phase of evolution, the instantaneous surface circulation changes significantly from the initial spin-up phase (Fig. 4a), developing instabilities and a vigorous mesoscale eddy field. An example of the instantaneous flow field during this fully developed phase is shown in Fig. 4b, after approximately 6 months of integration. Time averages of the circulation, on the other hand (computed every 3 and 6 months), do not show significant changes after the first 3 months, maintaining a quasi-stationary pattern.

The surface average velocity in experiment DG1 is shown in Fig. 6a. The MAW flows eastward from the western box, roughly following the topography along the Tunisian shelf. At the Channel level, branching of

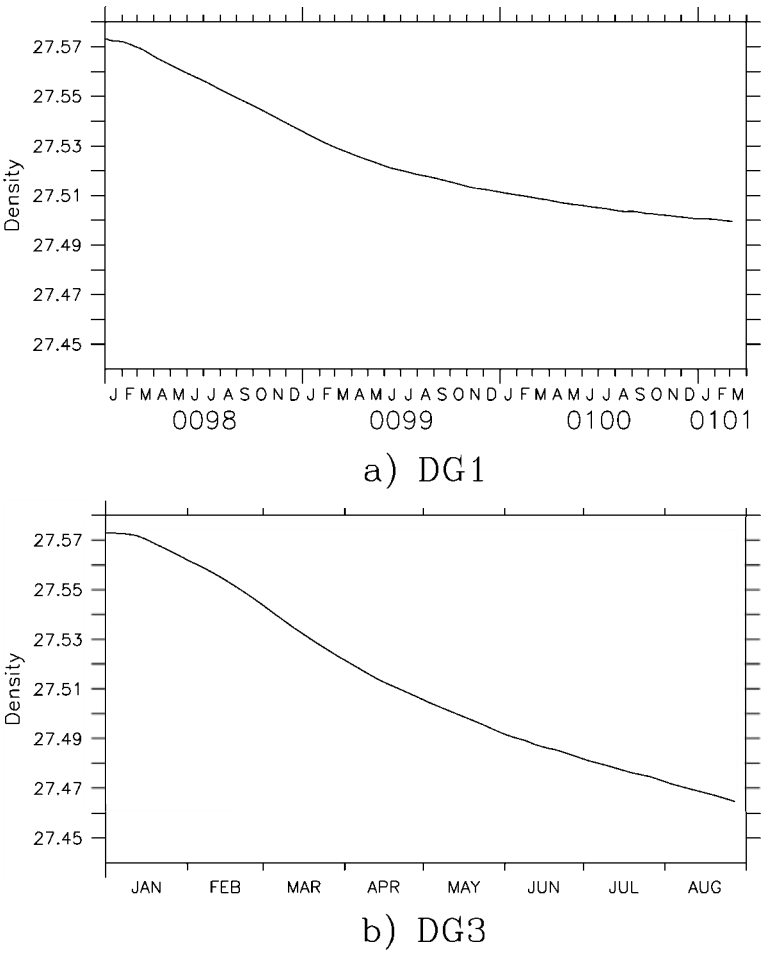

Fig. 5. Time evolution of basin-integrated density $\rho_D(t)$ calculated for $D=15$ m (a) for the experiment DG1 and (b) for the experiment DG3.

the flow takes place, similarly to that shown in the spin-up solution (Fig. 4a). One branch crosses the Channel and continues eastward in the Tyrrhenian Sea along the northern coast of Sicily, while two other branches enter the Channel, the main branch flowing southward along the Tunisian coast and a secondary branch along the western coast of Sicily. The Tunisian branch appears to later cross the Channel to join the Sicily coast north of Malta. The joint current then flows northward in the Ionian Sea following the coast.

The structure of the simulated velocity field is qualitatively similar to the observed AIS pattern (Fig. 1a). The magnitudes of velocities, however, are significantly lower than the observations, approximately by a factor of 3.

Next, the effect of increasing the density difference $\Delta\rho$ on the circulation patterns is studied by considering the results from experiments DG2 and DG3. The experiments DG2 and DG3 are integrated for a shorter time than the experiment DG1, for 6 and 8 months, respectively. This is partially justified by the fact that the time evolution in these experiments is expected to be faster, since the advection velocity scales are larger for DG2 and DG3 than for DG1. A bulk estimate of the change in advection velocity as function of $\Delta\rho$ is provided by the transport values in the three experiments (see Section 3.4 and Table 2). They suggest a roughly linear increase of advection velocity with $\Delta\rho$, with a factor ≈ 2 and 3 with respect to DG1 for DG2 and DG3, respectively. If the time scale of evolution is

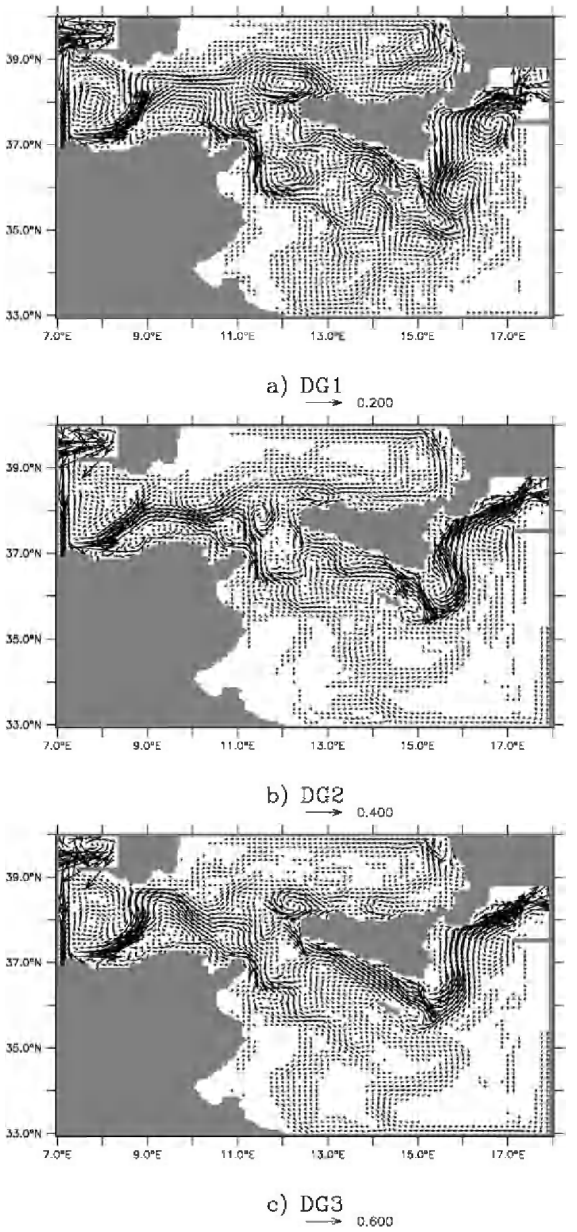

Fig. 6. Time-averaged surface circulation (in m s^{-1}) for the experiments (a) DG1 (averaged over 2 years), (b) DG2 (averaged over 6 months) and (c) DG3 (averaged over 8 months).

assumed to be inversely proportional to the advection velocity scale, this suggests 2 (3) times shorter time scales for DG2 (DG3) with respect to DG1. This is in qualitative agreement with the time evolution of $\rho_D(t)$ (defined in Eq. (1)) for DG3 (Fig. 5): $\rho_D(t)$ in DG3 has a similar behaviour to that from DG1, but with a time scale approximately 3 times faster (analogous results are obtained for DG2, with a corresponding factor of 2).

During this phase, the instantaneous velocity field in DG3 (and DG2) is unstable as in DG1, as illustrated by the snapshot at $t=6$ months in Fig. 4d. Also as in DG1, the time averages of the velocity field do not change significantly (after the first month period), suggesting that the velocity statistics is quasi-stationary even though the density field is still evolving. Fig. 6b,c show the average velocity fields for DG2 and DG3 performed over the whole integration period, starting at $t=1$ month.

The surface velocity structure (Fig. 6a–c) is qualitatively similar in the three experiments, showing similar branching at the Channel entrance and the characteristic AIS pattern. At a more detailed level, though, differences can be noticed, especially regarding the southward Sicilian current. The relative strength of this current appears to intensify at increasing $\Delta\rho$, i.e. at increasing nonlinearity. One possible explanation for this behavior is that the incoming MAW tends to mix more vigorously and rapidly at increasing nonlinearity, and this leads to a decrease in the associated density gradient. As shown in Section 3.1, the MAW density gradient is primarily associated with the branching and setting of the Tunisian southward current. As a consequence, the decrease in the MAW gradient results in a weakening of the Tunisian current and a relative strengthening of the Sicilian current.

Time-averaged circulation patterns at the intermediate level (350 m) are depicted in Fig. 7. In DG1, the velocity field at this level (Fig. 7a) is found to have a structure qualitatively similar to the observed pattern (Fig. 1b), but the velocity values are smaller, as for the surface circulation. The main current enters the Channel through the eastern sill, close to the Sicilian shelf, flowing toward the northwest. After exiting the western side of the Channel, the current flows mostly eastward following the Tyrrhenian shelf. This circulation pattern is similar in the three experiments, suggesting a weaker dependence on nonlinearity with respect to the surface velocity. This is not surprising given the stronger topographic constraint, especially inside the Channel area. The most noticeable difference between the experiments

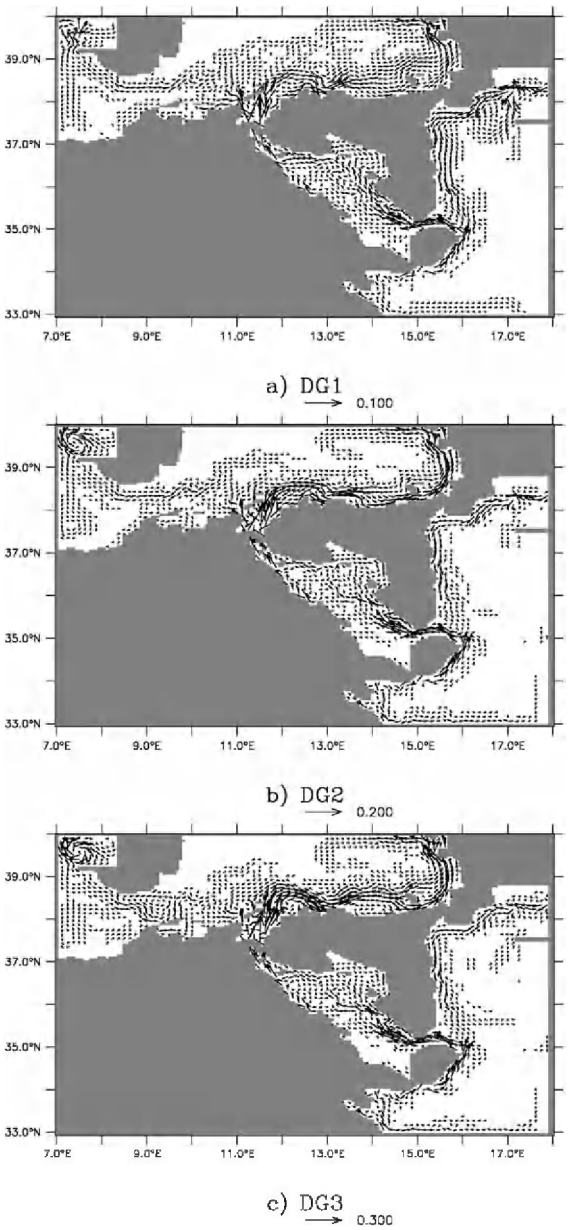

Fig. 7. Time-averaged intermediate level (350 m) circulation (in m s^{-1}) for the experiments (a) DG1, (b) DG2 and (c) DG3.

takes place outside the Channel, in the eastward Tyrrhenian current, which becomes stronger with increasing $\Delta\rho$ (Fig. 7a–c) in a consistent manner with the increased Tyrrhenian transport discussed above.

A qualitative validation of the model can be obtained comparing model and in-situ observations of property distribution. In Fig. 8, the salinity S distribution at a section across the Channel from the experiment DG1 at $t=3.5$ years is compared to that from in-situ data. While the realistic salinity values are not reproduced in the model simulation, since the solution is not yet at equilibrium and still depends on the choice of the initial values (especially for the LIW, see Table 3), the spatial structure of the isolines appears to be in good agreement with that from observations. The vertical and horizontal structure of the two main water masses (MAW at the surface and LIW at intermediate level), and their core positions are satisfactorily reproduced by the model. The S minimum occurs in the surface level. Its core (indicative of the MAW) is found near to the Tunisian coast, and it weakens toward the sicilian coast. Maximum salinity values, instead, are indicative of the presence of LIW water and are found in the intermediate level. LIW water is found predominantly in the eastern part of the basin, closer to the sicilian coast. The similarity between S patterns in model and data suggests that also the underlying velocity structure of the model is realistic. Whether the model is capable of reproducing realistic features because of its internal model dynamics or because of the constraints imposed by the boundary conditions is a question that cannot be answered at this point, as for any regional model.

3.3. Water mass advection

The advection of the MAW is first studied qualitatively following the spreading in time of its signature in terms of lighter density water. Density maps at 3-month intervals from the beginning of the experiment DG1 are shown in Fig. 9, providing a direct visualization of the main paths of advection. At $t=3$ months (Fig. 9a), the MAW reaches the Channel, while by $t=6$ months (Fig. 9b), the branching in the velocity field clearly influences the density distribution. Two main low-density branches are evident, one entering the Channel along the Tunisian shelf and the other crossing the Channel into the Tyrrhenian Sea. There is also an indication of a third branch flowing in the Channel following the western Sicilian coast. In the following months (Fig. 9c), a progressive southwestward motion of the MAW is observed in the Channel, developing patterns similar to the observed AIS (Robinson et al., 1999; Malanotte-Rizzoli et al.,

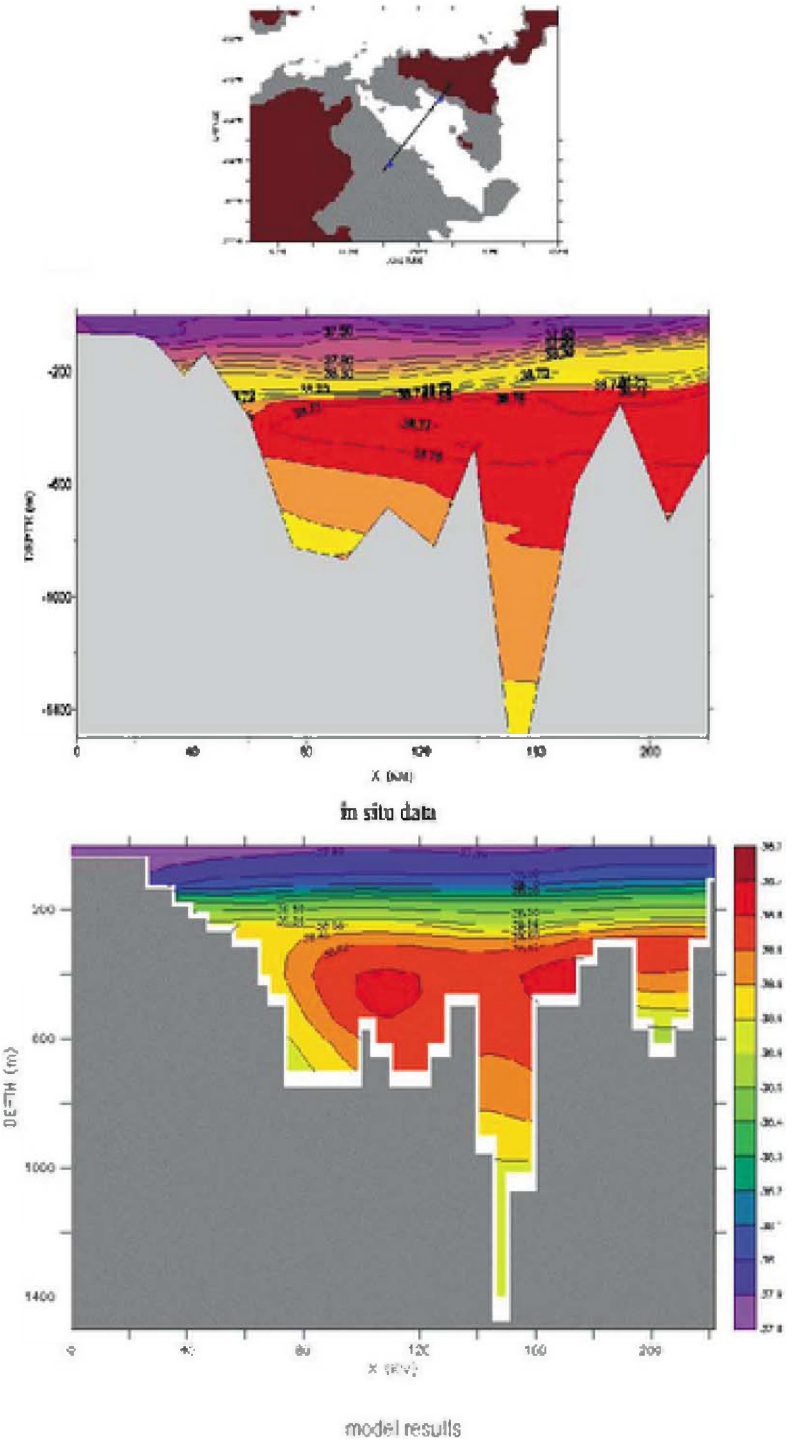

Fig. 8. Salinity distributions (in psu) at a section across the Sicily Channel from in-situ data (MATER2 Cruise, January 1997) and from the experiment DG1.

Table 3
Salinity values in the surface, intermediate and bottom layers for experiment DG1

Box1	Interior	Box2
37.5	38	38.5
38.5	38.5	39
38.75	38.75	38.75

The "box" salinities are kept fixed, whereas the "interior" salinity corresponds to that at the initial time. The thicknesses of the surface, intermediate and bottom layers are 150, 450, and 3500 m, respectively.

1997). At $t=1$ year (Fig. 9d), the MAW reaches the Ionian Sea (corresponding to the significant decrease of the slope of ρ_D in Fig. 5). After 2 years of integration (not shown) the MAW reaches the eastern wall, where the buffer zones maintain the density gradient.

As a next step, some more detailed and quantitative questions are considered about MAW advection. Observations (Sparnocchia et al., 1999; Astraldi et al., 1996) show that at the entrance of the Channel, minimum density values are found close to Tunisia. This suggests that the Tunisian branch is the most effective one in transporting the MAW, while the role of the current along the Sicily coast in advecting MAW it is not entirely clear.

In order to explore these issues using the model results and in order to obtain a more quantitative picture of MAW advection, the time series of $\rho(t)$ at four different points in the domain are computed. Notice that model results, strictly speaking, cannot be directly compared to observation, since the solution is still evolving and the results cannot be considered as representative of "typical" MAW pathways.

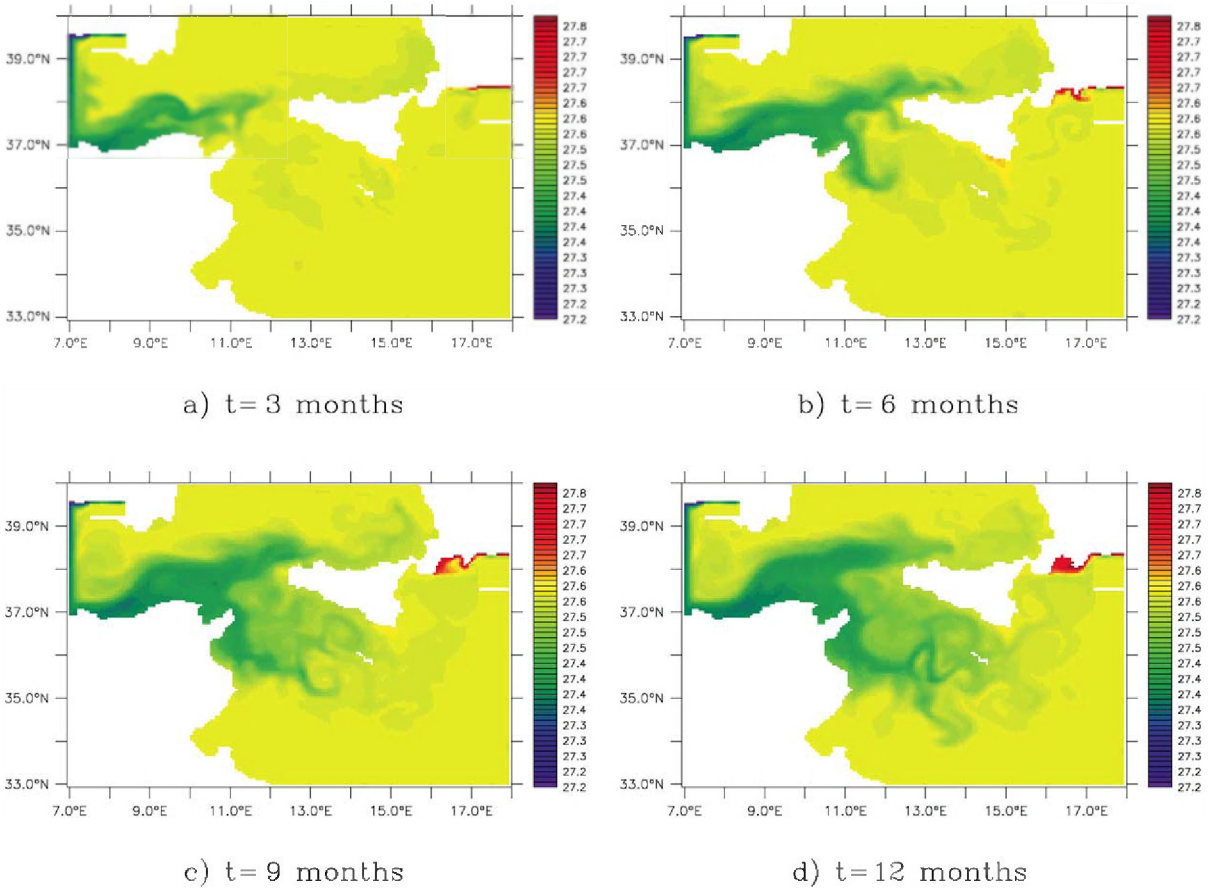

Fig. 9. Snapshots of surface density ($\sigma=\rho-1000$ in kg m^{-3}) in the experiment DG1 at (a) 3, (b) 6, (c) 9 and (d) 12 months.

Nevertheless, the spin up process is useful to understand the mechanisms of advection and mixing, and it can be used to understand tendencies in the solution. The four points of measurements, M1, M2, M3, M4, are indicated in Fig. 2. The point M1 is located north of the Tunisian coast, outside from the Channel. The points M2 and M3 are inside the Channel, close to the Tunisian and Sicilian coasts, respectively, while the point M4 is located in the Tyrrhenian Sea. In all cases, the density $\rho(t)$ is computed at the surface level, where the low density signal is more evident.

The results from experiment DG1 (Fig. 10a) show that the highest and most stable signal of the MAW advection is present at point M1. This is expected since M1 is the closest point to the source and it is located upstream of the Channel bifurcations. The effect of the incoming MAW starts after 2 months of integration and reaches an equilibrium value (density minimum) after approximately 1 year. This value is approximately the average between the initial value and the density value of the water from the Atlantic box (see Table 1). For the other points, greater variability in the evolution of density is present, probably due to higher mesoscale variability. Despite this, a clear arrival signal for the MAW can be noticed at all points, characterized by a sharp decrease of $\rho(t)$.

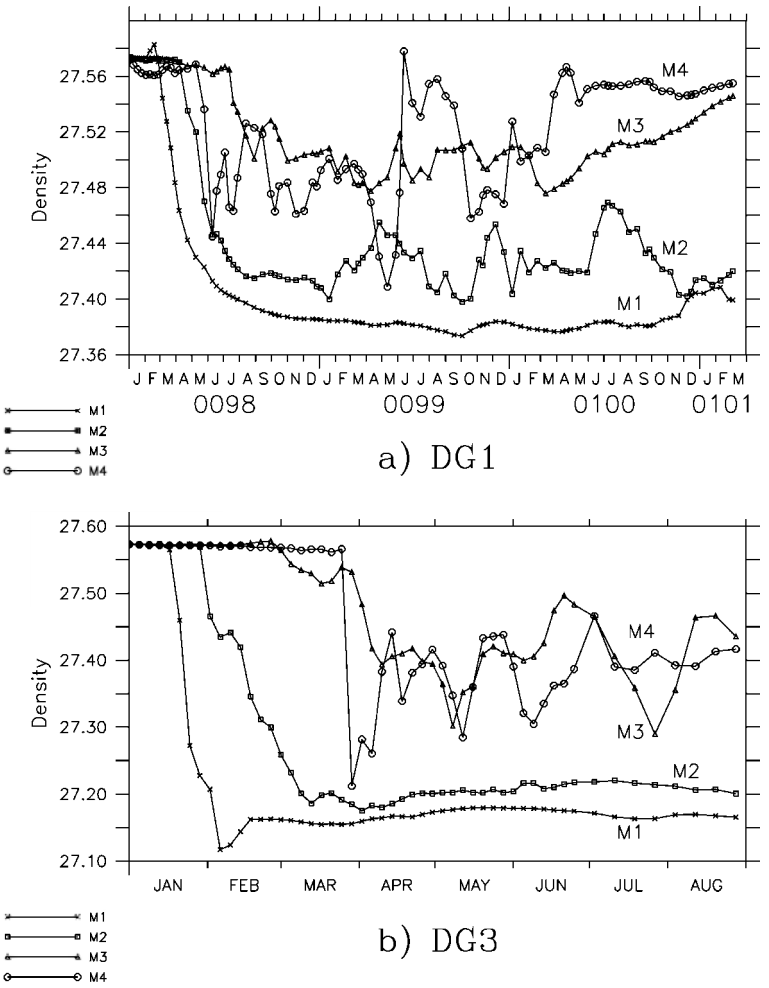

Fig. 10. Evolution of density ($\sigma = \rho - 1000$ in kg m^3) in time at the locations M1, M2, M3, M4 (see Fig. 2) in the experiments (a) DG1 and (b) DG3.

The first point reached by the MAW after M1 is M2 (at $t \approx 3$ months), where also the lowest density value at equilibrium is found. This indicates that the main incoming path of the MAW into the Channel is indeed along the Tunisian coast. Next arrival times occur at M4 (at $t \approx 4$ months) and then at M3(at $t \approx 6$ months). The density values in the two points are qualitatively similar (aside from strong fluctuations at M4), and they are distinctively higher than those at M2. This suggest that while the MAW advection is confirmed at both points, the density signal is weaker because of more extensive mixing. Also, it is possible that the water advected in the Channel along the Sicilian coast is partially recirculating in the Tyrrhenian Sea before entering the Channel, as suggested by the later arrival and similar mixing.

The results in regards to the advection of MAW using the surface density evolution $\rho(t)$ at the points M1–M4 from the experiment DG3 are shown Fig. 10b. As in the experiment DG1, the fastest and clearest signal of the MAW advection is found at point M1 (at $t \approx 15$ days), and a few days later at M2. The equilibrium value of the density at these points is $\sigma = \rho - 1000 \approx 27.2$. Note that the density is relatively higher than the average between the initial condition value and the value of the incoming Atlantic water, suggesting a more vigorous mixing close to the box, as discussed above. As in DG1, the density at points M3 and M4 are very similar and higher than that at point M2.

Similar results are found in the experiment DG2 (not shown) to those in DG1 and DG3, confirming that the incoming MAW is advected in the Channel and splits into three main branches and that the stronger signal is always present in the branch along the Tunisian coast.

3.4. Transport

Transport time series of the surface MAW (Fig. 11) are computed across the two vertical closed sections shown in Fig. 2: Section S1 is across the Sardinia Channel between Tunisia and Sardinia, and Section S2 is across the Sicily Channel between Tunisia and Sicily. Transport across S1, denoted T_{S1}, characterizes the MAW mass flux entering the domain, while transport across S2, T_{S2}, quantifies the mass flux across the Channel. Using T_{S1} and T_{S2}, an estimate can be obtained also for the transport entering the Tyrrhenian Sea, $T_{S3} = T_{S1} - T_{S2}$, which is not estimated directly because the section cannot be closed correctly at the northern boundary of the domain, which is artificially closed by a buffer zone characterized by a weak return flow (see Fig. 4). Note that, due to the rigid-lid assumption, the net volume transport across the Channel, integrated over the whole water column, has to be zero at all times. Consequently, the transport in the two layers (MAW and LIW) is equal and opposite.

The transport calculation is done according to the definition

$$T = \int_L \mathrm{d}l \int_0^{-DV} \mathrm{d}z \boldsymbol{v}\dot{\boldsymbol{n}} \tag{2}$$

where L is the section, $\boldsymbol{n}$ is the unit vector normal to the section, $\boldsymbol{v}$ is the horizontal velocity vector and DV is the depth at which $\boldsymbol{v}\dot{\boldsymbol{n}}$ changes sign in average.

The results for the time series T_{S1} and T_{S2} from the experiment DG1 are shown in Fig. 11a and are summarized in Table 2 in terms of mean and standard deviation (s.d.). The parameter DV in Eq. (2) has been chosen by analyzing isopycnals and velocity distributions in the vertical sections, in order to obtain an estimate of the averge interface depth. Sensitivity to the DV values has been tested over a wide range, and this parameter was chosen in order to obtain the highest and most stable transport across a specific section (as the MAW structure can change depth during its route). The values of this parameter are taken as $DV = 200$ m for T_{S1} and $DV = 150$ m for T_{S2}. As can be seen in Fig. 11a and Table 2, the time series becomes quite regular after the first adjustment phase of approximately 1 month, with s.d. on the order of 12–21% with respect to the mean. Strictly speaking, since the solution is still evolving, the mean transport values cannot be considered as definitive and significant of the equilibrium solution. On the other hand, given the absence of obvious trends, we can assume that they can be used to at least provide qualitative estimates of the transport properties in the area.

The mean transport values in experiment DG1 are 0.47 Sv for T_{S1}, and 0.31 Sv for T_{S2}, suggesting a Tyrrhenian Sea transport T_{S3} of ≈ 0.16 Sv. The transport T_{S2} across the Sicily Channel appears significantly smaller (of approximately a factor 1/3) than

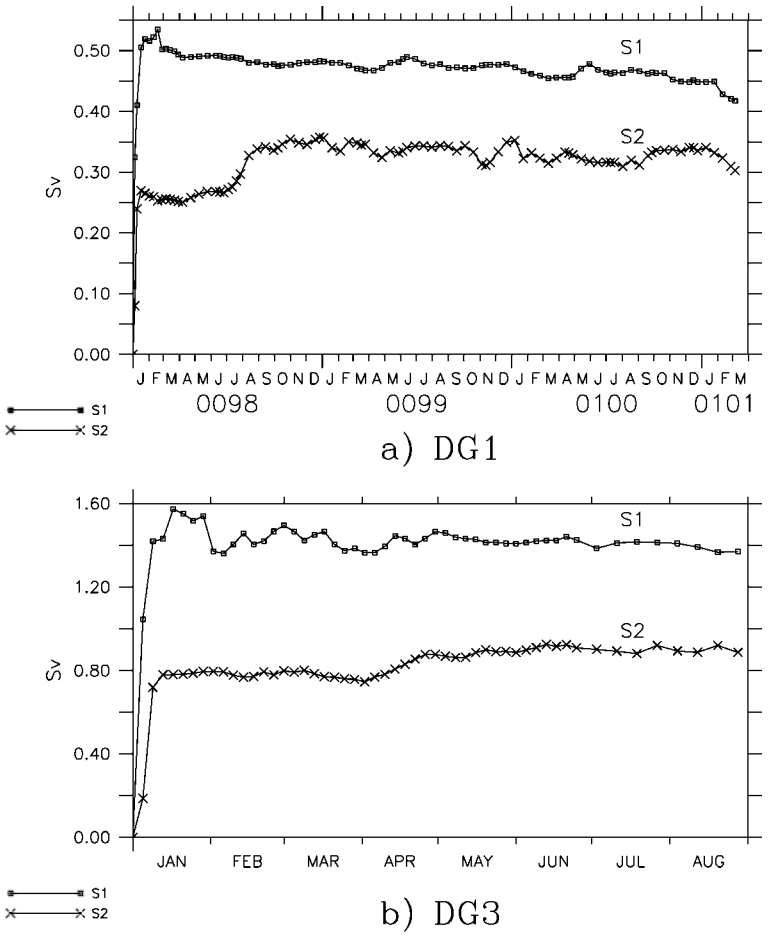

Fig. 11. Volume transport (in Sv) computed across sections S1 and S2 in the experiments (a) DG1 and (b) DG3.

both the values estimated from observations (Astraldi et al., 1999), and the values obtained by the thermohaline calculations (Bethoux, 1979). However, the ratio of the Channel and Tyrrhenian transports, T_{S3} and T_{S2}, with respect to the total entering MAW transport, T_{S1}, i.e. T_{S3}/T_{S1} and T_{S2}/T_{S1} are approximately 1/3 and 2/3, respectively, in good agreement with the observed ratios of these transports.

Transport time series for DG3 are shown in Fig. 11b, while the statistics for both DG2 and DG3 are summarized in Table 2. As in DG1, a rapid increase is observed during the first 1–2 weeks, in correspondence to the setting of the circulation associated with the Kelvin front propagation. At $t \approx 1$–2 months, a quasi-equilibrium is reached. The average transport values (Table 2) increase with $\Delta\rho$, in an approximately linear fashion. The standard deviations for both sections are in the same range for the three experiments, even though some quantitative differences can be noticed. Mean transport values for the cross Channel transport T_{S2} are 0.53 Sv in DG2, and 0.81 Sv in DG3.

Estimates of mean transport in the Tyrrhenian Sea, T_{S3} yield 0.39 and 0.58 Sv in DG2 and DG3, respectively. The ratios T_{S2}/T_{S1} and T_{S3}/T_{S1} are slightly different from those in DG1 (see Table 2) and suggest an increased Tyrrhenian transport. With respect to the total MAW flux T_{S1}, T_{S3} appears larger (of approximately 25%) than the 1/3 value suggested by the data, even though the significance of this result might be questionable, given the high estimate error.

4. Transport estimates using the steric height difference method

In this section, the estimates of cross-Channel transport, T_{S2}, obtained from the numerical model in Section 3.4 are compared with other estimates obtained using a simplified "bulk" method, i.e. the method of steric height differences (e.g. Hopkins, 1999). The method, briefly described in the following, estimates the mean exchange through a strait connecting two adjacent basins without explicitely resolving the details of the flow in the strait, but rather assuming some simplifying assumptions such as geostrophy for the low frequency component of the flow (Garrett and Toulany, 1982). The comparison with the T_{S2} estimates of Section 3.4 allows to verify whether or not these assumptions can be considered valid and wether or not the method can be correctly applied to the Channel. If this is the case, the method can then be used to explore the sensitivity of the transport T_{S2} to density differences not covered by the numerical experiments. In particular, we are interested in exploring the sensitivity to density differences in the intermediate layer, which have been neglected in the numerical experiments.

The geostrophic flow in a strait can be written in terms of pressure difference between the two adjacent basins (Garrett and Toulany, 1982):

$$u_g = -\frac{\Delta P}{\rho f W}, \tag{3}$$

where u_g is the current through the strait, ΔP is the pressure gradient between basins, f is the Coriolis parameter and W is the width of the strait.

Following Hopkins (1999) we can separate the total pressure P in its barotropic and baroclinic component (indicated by suffix "bt" and "bc", respectively) and express them as follows:

$$P(z) = P_{\mathrm{bt}} + P_{\mathrm{bc}}(z) = \rho_0 g \zeta_{\mathrm{bt}} + g \int_0^z \rho(z)\mathrm{d}z \tag{4}$$

where ζ_{bt} is the sea level and ρ_0 is the surface density. By subtracting a reference pressure $P_{\mathrm{r}} = \rho_{\mathrm{r}} g z$ from both sides of Eq. (4), P_{bc} can be expressed in terms of the steric height parameter ζ_{sh},

$$P(z) - P_{\mathrm{r}} = g\rho_0(\zeta_{\mathrm{bt}} - \zeta_{\mathrm{sh}}(z))$$

where $\zeta_{\mathrm{sh}} = 1/\rho_0(\rho_{\mathrm{r}} - \bar{\rho}(z))z$ and $\bar{\rho}(z) = \frac{1}{z}\int_0^z \rho(z)\mathrm{d}z$

The geostrophic flow of Eq. (3) can then be written as:

$$u_g = -\frac{g}{fW}(\Delta\zeta_{\mathrm{bt}} - \Delta\zeta_{\mathrm{bc}}(z))$$

The conservation of volume transport imposes the balance between barotropic and baroclinic components and the equivalence between upper-layer inflow and lower-layer outflow. As a consequence, the fluxes through the strait can be estimated directly, when the profiles $\rho(z)$ in the two basins are known and the term $\Delta\zeta_{\mathrm{bc}}$ is computed.

Here, the steric height method is applied in correspondence of the western sill of the strait of Sicily, assuming the same section area used in the model. Geometric characteristics of the section are the maximum surface width of 140 km in the first 100 m and maximum depth of 350 m. The same layer structure as in the experiment "boxes" are considered. This implies that the adjacent basins are connected by a section of ≈ 15 km^2 in the surface layer and only by a section of ≈ 6 km^2 in the second layer. There is no connection for the deepest layer.

Assuming the previous geometric characteristics, estimates of the transport though the strait have been computed for the three profiles in Table 1. For the DG1 case ($\Delta\rho = 0.77$), a transport of ≈ 0.34 Sv is found, with the mean depth of the interface at about 92 m. Increasing density gradient ($\Delta\rho = 1.53$ and 2.30), the transport increases to 0.53 Sv for DG2 and 0.86 Sv for DG3. As can be seen, the values for the three cases agree well with the mean T_{S2} values of Section 3.4, with differences smaller than the s.d. (Table 2). This indicates that the simplified method is valid in the range of the considered values.

Next, we consider the case of density differences also in the second layer, which are neglected in Section 3. As done in Section 2 for the surface differences, the intermediate density difference, $\Delta\rho_{\mathrm{I}}$, is assigned considering climatological density values (Brasseur et al., 1996; Guibout, 1987) occurring at ≈ 350 m in the two basins connected by the Channel. Differences in the neighbouring regions (as in DG1) are found to be negligible, while for the far field (as in DG3) they are found to be $\Delta\rho_{\mathrm{I}} \approx 0.05$. The corresponding transport turns out to be ≈ 0.87 Sv, with only 0.01 SV difference with the case with $\Delta\rho_{\mathrm{I}} = 0$.

This indicates that the density differences in the intermediate layer can be neglected, providing therefore an a-posteriori validation to the results of Section 3. The reason is due to the particularly narrow passage below 200 m of depth, which allows the pressure effect of deeper layers to act only in few points of the passage.

5. Summary and concluding remarks

The remotely forced density-driven component of the circulation in the Sicily Channel has been investigated considering a simplified setting, in which the forcing is provided by density differences along the Channel. Two "boxes" with given density profiles are set at the two opposite sides of Channel, representing the action of the two sub-basins connected by the Channel. A range of density values for the boxes (and corresponding density differences $\Delta\rho$ along the Channel) are considered. Three main values of $\Delta\rho$ characteristic of the surface layer are considered, $\Delta\rho = 0.77$, 1.53, 2.30, corresponding to experiments DG1, DG2 and DG3, respectively. The lowest value corresponds to $\Delta\rho$ based on climatological density value in the neighbouring regions (Sardinia Channel and Ionian Sea), while the highest values correspond to more remote density values, i.e. to differences between the far-field western and eastern Mediterranean sub-basins. The action of density differences in the intermediate layers is investigated using the steric height method and found negligible.

The experiments are characterized by a first, rapid spin-up phase characterized by the propagation of Kelvin fronts, followed by a longer spin-up phase related to the water mass advection in the domain. Even though the density field is still evolving at the end of the integration, the average velocity fields appear statistically stationary, while transport estimates across the main sections appear approximately constant in time. This suggests that the results can be considered at least qualitatively indicative of the circulation in the domain. These qualitative estimates might be still influenced by other numerical factors, such as the simplified boundary condition.

The patterns of the average circulation and of water mass advection maintain qualitatively similar characteristics at varying $\Delta\rho$. Regarding the LIW, the circulation is almost unchanged, and it is consistent with measurements. The salinity core in the Channel is found closer to the Sicilian shelf and vertical sections are similar to data. After exiting the Strait, the LIW is mostly advected in the Tyrrhenian Sea, in agreement with experimental data (Astraldi et al., 1996). Regarding the MAW, the simulated circulation captures many of the observed features. The incoming MAW branches at the Strait level, with one branch entering the Strait and flowing southward along the Tunisian coast, while the other branch crosses the Strait and enters the Tyrrhenian Sea. A secondary branching and the formation of a southward Sicilian current is also observed. The patterns of the AIS are present, with the current crossing the Channel north of Malta and roughly following topography moving northward along the Sicilian coast in the Ionian Sea. The experiment results indicates that the strength of the incoming eastern flux of MAW and its branching at the Strait level with subsequent formation of the Tunisian current are mostly controlled by the density differences with the eastern sub-basin. The strength of the AIS stream, and its northern flux in the Ionian Sea along the Sicily coast, instead, are controlled by the density differences with the western sub-basin.

The transport across the Channel is found to increase approximately linearly with $\Delta\rho$, with mean values of $T_{S2} \approx 0.3$ Sv in DG1 and $T_{S2} \approx 0.8$ Sv in DG3. For all the experiments, the ratios of the Tyrrhenian (T_{S3}) and cross Channel (T_{S2}) transports with respect to the MAW transport (T_{S1}) are in a similar range and in approximate agreement with the observations: $T_{S3}/T_{S1} \approx 1/3$ and $T_{S2}/T_S \approx 2/3$. For the experiments DG2 and DG3, though, T_{S3}/T_{S1} appears slightly larger than 1/3, suggesting an increased Tyrrhenian transport. Also, for increasing $\Delta\rho$, the Sicilian MAW branch in the Channel appears to intensify with respect to the Tunisian branch. It is suggested that this is an effect of nonlinearity, related to increased mixing in the MAW resulting in a relative weakening of the Tunisian branch.

In summary, the results suggest that density currents in the considered range of $\Delta\rho$ are characterized by a number of features similar to the observed ones in the Channel, while the transport through the Channel varies almost linearly with $\Delta\rho$, ranging between 0.3 and 0.8 Sv.

Obviously, there is also a number of observed aspects of the circulation that are not captured in the simulations, and they are likely to be related to different forcings. Measured transports show standard deviations and instaneous values which are significantly higher than the simulated transports. This is almost certainly related to direct wind forcing. Also, some current features appear to have different properties in the model and in the observations. For example, the southward Tunisian current entering the Channel is very stable in the model and never leaves the coast, while a much stronger variability is suggested by drifter observations (Poulain and Zambianchi, personal communication). This may be due to the lack of direct wind effect or to instabilities of the incoming current that are not correctly reproduced by the simple model. Finally, we point out that upwelling close to the Sicilian coast in the Channel is not present in the model, while it is frequently observed in in-situ data. This phenomenon is certainly related to local wind forcing as well.

Acknowledgements

This work has been supported by the Office of Naval Research under grant N00014-97-1-0620, and by the EC-Mast Project MATER under grant MAS3-CT96-0051. The authors gratefully thank M. Crepon and A. Vetrano for useful discussion and suggestions.

References

Andrich, P., Delecluse, P., Levy, C., Madec, G., 1988. A multitasked ocean general circulation model of the ocean. Science and Engeineering on Cray Supercomputers, Proceed. of the Fourth International Symposium, Cray Research, pp. 407–428.

Astraldi, M., Gasparini, G.P., Sparnocchia, S., Moretti, M., Sansone, E., 1996. The characteristics of water masses and the water transport in the Sicily Strait at long time scales. Bull. Inst. Oceanogr. (Monaco) 17, 95–115.

Astraldi, M., Balopoulos, S., Candela, J., Font, J., Gacic, M., Gasparini, G.P., Manca, B., Theocharis, A., Tintore, J., 1999. The role of straits and channel in understanding the characteristics of Mediterranean circulation. Prog. Oceanogr. 44, 65–108.

Bethoux, J.P., 1979. Budgets of the Mediterranean Sea. Their dependence on the local climate and on the characteristics of the Atlantic waters. Oceanol. Acta 10, 157–163.

Brasseur, P., Beckers, J.M., Brankart, J.M., Shoenauen, R., 1996. Seasonal temperature and salinity fields in the Mediterranean Sea: climatological analyses of a historical data set. Deep-Sea Res. 43 (2), 159–192.

Garrett, C., Toulany, B., 1982. Sea-level variability due to meteorological forcing in the North-east Gulf of St. Lawrence. J. Geophys. Res. 87, 1968–1978.

Garzoli, S., Maillard, C., 1979. Winter circulation in the Sicily and Sardinia Straits region. Deep-Sea Res. 26A, 933–954.

Gervasio, L., Mortier, L., Crepon, M., 2002. The Sicily Strait dynamics. A sensitivity study with a high resolution numerical model. J. Phys. Oceanogr. (submitted for publication).

Guibout, P., 1987. Atlas hydrologique de la Mediterranee. Editions Ifremer/Shom, Paris.

Heburn, G.W., 1994. The dynamics of the seasonal variability of the western Mediterranean circulation. In: La Violette, A. (Ed.), Coast. Estuar. Stud., vol. 46, pp. 249–285. AGU.

Herbaut, C., Mortier, L., Crepon, M., 1996. A sensitivity study of the general circulation of the Western Mediterranean: Part I. The response to density forcing through the Straits. J. Phys. Oceanogr. 26, 65–84.

Herbaut, C., Codron, F., Crepon, M., 1998. Separation of a coastal current at a strait level: case of the Strait of Sicily. J. Phys. Oceanogr. 28, 1346–1362.

Hopkins, T.S., 1999. The thermohaline forcing of the Gibraltar exchange. J. Mar. Syst. 20, 1–31.

Horton, C., Clifford, M., Schmitz, J., 1997. A real-time oceanographic now-cast/forecast system for the Mediterranean Sea. J. Geophys. Res. 102, 25123–25156.

Korres, G., Pinardi, N., Lascaratos, A., 2000. The ocean response to low-frequency inter annual atmospheric variability in the Mediterranean Sea: Part I. Sensitivity experiments and energy analysis. J. Clim. 13 (4), 705–731.

Madec, G., Chartier, M., Crepon, M., 1991a. Effect of thermohaline forcing variability on deep water formation in the Western Mediterranean Sea: a high resolution three dimensional numerical study. Dyn. Atmos. Ocean. 15, 301–332.

Madec, G., Chartier, M., Delecluse, P., Crepon, M., 1991b. Numerical study of deep-water formation in the northwestern Mediterranean Sea. J. Phys. Oceanogr. 21, 1349–1371.

Malanotte-Rizzoli, P., Manca, B.B., Ribera d'Alcala, M., Theocharis, A., Bergamasco, A., Bregant, D., Budillon, G., Civitarese, G., Georgopoulos, D., Michelato, A., Sansone, E., Scarazzato, P., Souvermezoglou, E., 1997. A synthesis of the Ionian Sea hydrography, circulation and water mass pathways during POEM-Phase I. Prog. Oceanogr. 39, 153–204.

Manzella, G.M.R., Gasparini, G.P., Astraldi, M., 1988. Water exchange between the eastern and western Mediterranean through the Strait of Sicily. Deep-Sea Res. 35 (6), 1021–1035.

Manzella, G.M.R., Hopkins, T.S., Minnett, P.J., Nacini, E., 1990. Atlantic Water in the Strait of Sicily. J. Geophys. Res. 95, 1569–1575.

Moretti, M., Sansone, E., Spezie, G., De Maio, A., 1993. Results of investigations in the Sicily Channel (1986–1990). Deep-Sea Res. 40, 1181–1192.

Onken, R., Sellshop, J., 1998. Seasonal variability of flow instabilities in the Strait of Sicily. J. Geophys. Res. 103 (C11), 24799–24820.

Pacanowski, R.C., Philander, S.G., 1981. Parametrization of vertical mixing in numerical models of tropical oceans. J. Phys. Oceanogr. 11, 1443–1451.

Pierini, S., Rubino, A., 2001. Modeling the oceanic circulation in the area of the Strait of Sicily: the remotely-forced dynamics. J. Phys. Oceanogr. 31 (6), 1397–1412.

Pratt, L.J. (Ed.), 1990. The Physical Oceanography of Sea Straits. Kluwer Academic Publishers, Dordrecht.

Robinson, A.R., Sellshop, J., Warn-Varnas, A., Leslie, W.G., Lozano, C.J., Haley Jr., P.J., Anderson, L.A., Lermusiaux, P.F.J., 1999. The Atlantic Ionian Stream. J. Mar. Syst. 20, 129–156.

Sparnocchia, S., Gasparini, G.P., Astraldi, M., Borghini, M., Pistek, P., 1999. Dynamics and mixing of the Eastern Mediterranean outflow in the Tyrrhenian basin. J. Mar. Syst. 20, 301–317.

Speich, S., Madec, G., Crepon, M., 1996. A strait outflow circulation process study: the case of the Alboran Sea. J. Phys. Oceanogr. 26, 320–340.